ACS APPLIED MATERIALS & INTERFACES

Research Article

www.acsami.org

Unsymmetrical Donor−Acceptor−Acceptor−π−Donor Type Benzothiadiazole-Based Small Molecule for a Solution Processed Bulk Heterojunction Organic Solar Cell

Prabhat Gautam,[†] Rajneesh Misra,*[,†] Shahbaz A. Siddiqui,[‡] and Ganesh D. Sharma*[,§]

[†]Department of Chemistry, Indian Institute of Technology, Indore, Madhya Pradesh 452017, India

[‡]Department of Electrical Engineering, Vivekanand Institute of Technology, Jagatpura, Jaipur, Rajasthan 302025, India

[§]R and D Center for Science and Engineering, JEC Group of Colleges, Jaipur Engineering College Campus, Kukas, Jaipur, Rajasthan 302028, India

Supporting Information

ABSTRACT: A D1−A−A′−π−D2 type (D = donor; A = acceptor) unsymmetrical small molecule denoted as BTD3 containing different end group donor moieties has been designed and synthesized for use as a donor in the solution processable bulk heterojunction (BHJ) solar cell. The BTD3 exhibits a low HOMO−LUMO gap of 1.68 eV and deeper HOMO energy level (−5.5 eV). Its LUMO energy level (−3.65 eV) is compatible with the LUMO level of $PC_{71}BM$ to facilitate the electron transfer from BTD3 to $PC_{71}BM$ in the BHJ solar cell. The solution processed BHJ solar cell with optimized BTD3:$PC_{71}BM$ active layer processed with THF solvent exhibited a PCE of 3.15% with J_{sc} = 7.45 mA/cm^2, V_{oc} = 0.94 V, and FF = 0.45. Moreover, the device with optimized concentration of 3 vol. % 1-chloronaphthalene (CN) additive, i.e., CN/THF, showed significant enhancement in PCE up to 4.61% (J_{sc} = 9.48 mA/cm^2, V_{oc} = 0.90 V, and FF = 0.54). The improvement in the PCE has been attributed to the appropriate nanoscale phase separation morphology, balance charge transport, and enhancement in the light harvesting ability of the active layer.

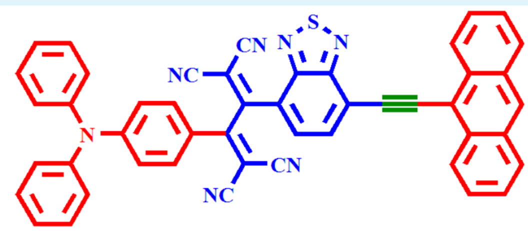

Active layer	PCE (%)
BTD3:$PC_{71}BM$ (processed with THF)	3.15
BTD3:$PC_{71}BM$ (processed with CN (3v%)/THF)	4.61

KEYWORDS: *unsymmetrical D1−A−A′−π−D2 small molecule, bulk heterojunction organic solar cells, power conversion efficiency, solvent additives*

1. INTRODUCTION

In recent years the power conversion efficiency of organic solar cells based on bulk heterojunction (BHJ) active layer comprised of electron donor (conjugated polymers or small molecules) and electron acceptor (fullerene derivatives) materials has increased remarkably and approached greater than 9%,[1−9] and are the potential candidate for a low cost commercial product.[10,11]

Organic BHJ solar cells based on a solution processed π-conjugated low bandgap small molecule as donor and fullerene derivatives as an acceptor have been investigated,[9,12−17] because of their advantages such as lightweight, flexibility, defined molecular structure, intrinsic monodispersity, high purity, negligible batch-to-batch variations, and reproducible performance, compared to conventional polymer counterparts.[18] The current research on organic solar cells focuses on the design and synthesis of new small molecules built by connecting various electron donating (donor) and electron withdrawing (acceptor) moieties through π-conjugated spacer (D−π−A).[19−26] The strength of the D−A interaction is determined by the donor and acceptor groups and the connecting π-bridges. It was reported that strong electron donating or accepting groups and long π-bridges tune the bandgap and assist the formation of favorable morphologies for high photovoltaic performance.[27] Li et al. and Chen et al. synthesized two-dimensional small molecules D2 and DR3TBDTT with an A−π−D−π−A framework and used as donor for solution processed BHJ organic solar cells which showed PCEs up to 6.75% and 8.12%, respectively.[22,28] The recent development on the solution processed small molecules BHJ solar cells has led to high PCEs of >8%.[29−32] In recent investigations, the PCE of the BHJ solar cells based on small molecules has been approaching 10%.[32−34]

We were interested in the design of a small molecule (SM) as donor material along with the $PC_{71}BM$ as electron acceptor for the fabrication of solution processed BHJ organic solar cells. The design of unsymmetrical BTD3 is based on the following considerations: (i) In D−A small molecules, an electron donating group such as triphenylamine (TPA) plays a significant role in stabilizing separated holes from excitons and improves the transport properties of the hole carrier.[35−37] Moreover, compounds containing a TPA unit as a donor end

Received: January 28, 2015
Accepted: April 24, 2015
Published: May 6, 2015

DOI: 10.1021/acsami.5b02250
ACS Appl. Mater. Interfaces 2015, 7, 10283−10292

unit were shown to exhibit an intense and broad absorption band that extends from UV to the far red end of the visible spectrum.[38,39] (ii) Anthracene and its derivatives have been widely investigated in organic field effect transistors (OFETs) in view of good hole mobilities as a result of $\pi-\pi$ stacking of adjacent molecules in films.[40,41] Anthracene-based D−A conjugated polymers have been also employed as donor for polymer BHJ solar cells and showed moderate PCE.[42−44] (iii) The 2,1,3-benzothiadiazole (BTD) is used as an acceptor owing to its high electron affinity. (iv) The incorporation of a tetracyanobutadiene (TCBD) unit results in tuning of the HOMO−LUMO gap of donor-substituted benzothiadiazoles.

Herein, we have synthesized a D1−A−A′−π−D2 type unsymmetrical small molecule denoted as BTD3 with D1 (TPA), A (TCBD), A′ (benzothiadiazole), π (ethynyl), and D2 (anthracene) and investigated its optical and electrochemical properties. A comparative representation of optical gaps of D−π−A−π−D, D1−π−A−π−D2, and D1−A−A′−D2 types of molecular motifs are shown in Chart 1, which reveal that the

Chart 1. Comparative Representation of Optical Gap of D−π−A−π−D, D1−π−A−π−D2, and D1−A−A′−D2 Types of Molecular Motifs.[46]

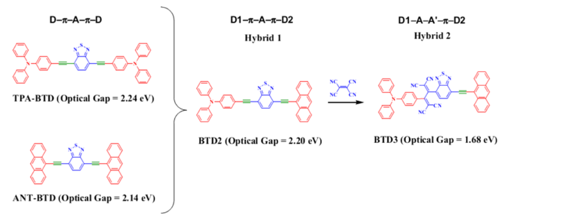

hybrid 2 (unsymmetrical BTD3) exhibits a low optical gap, which is desirable for BHJ organic solar cells. We have used BTD3 as donor material along with the $PC_{71}BM$ as electron acceptor for the fabrication of solution processed BHJ organic solar cells and showed moderate PCE (3.15% and 4.61% for the active layer processed with THF and CN/THF active layers, respectively). The higher PCE of the device processed with additive solvent was attributed to the more appropriate nanoscale morphology of the active layer and balanced charge transport, induced by the solvent additive.

2. EXPERIMENTAL SECTION

Device Fabrication and Characterization. The BHJ organic solar cells were prepared using indium tin oxide (ITO) coated glass substrate as anode, Al as cathode, and a blended film of BTD3:$PC_{71}BM$ between the two electrodes as photoactive layer, as follows: First, ITO coated glass substrates were cleaned with detergent, ultrasonicated in acetone and isopropyl alcohol, and subsequently dried in an oven for 12 h. An aqueous solution of PEDOT:PSS (Heraeus, Clevious P VP,Al 4083) in aqueous solution was spin-cast on the ITO substrates obtaining a film of about 40 nm thick. The PEDOT:PSS film was then dried for 10 min at a temperature of 120 °C in ambient conditions. Then, a 10 mg/mL solutions of BDT3/$PC_{71}BM$ blends in different solvents were prepared with different weight ratios and then spin-cast on top of the PEDOT:PSS layer and dried at 40 °C for 10 min in ambient atmosphere to remove the residue of the solvent. The solvents include THF and THF containing 1, 2, 3, and 4% (vol. %) CN. The thickness of the photoactive layer is about 100 ± 10 nm. Finally ~90 nm thick Al electrode was deposited on top of the BHJ film under reduced pressure ($<10^{-6}$ Torr). All of the devices were fabricated and tested in ambient atmosphere without encapsulation. The active area of the devices is about 0.20 cm^2.

The current−voltage characteristics of the devices were measured using a computer controlled Keithley 238 source meter in the dark as well as under illumination intensity of 100 mW/cm^2. A xenon light source coupled with AM1.5 optical filter was used as the light source to illuminate the surface of the devices. The incident photon to current efficiency (IPCE) of the devices was measured by illuminating the device through the light source and monochromator, and resulting current was measured using a Keithley electrometer under short circuit condition.

3. RESULTS AND DISCUSSION

Synthesis and Characterization of BTD3. The synthesis of unsymmetrical D1−A−A′−π−D2 small molecule denoted as BTD3 is shown in Scheme 1. The triphenyamine-substituted benzothiazole (1) was synthesized by the Pd-catalyzed

Scheme 1. Synthesis of BTD3

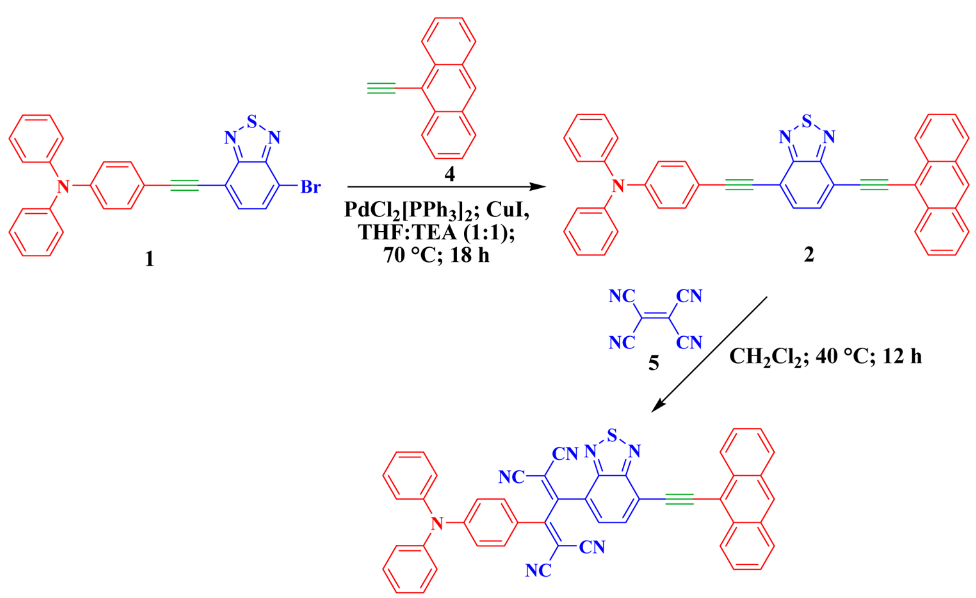

DOI: 10.1021/acsami.5b02250
ACS Appl. Mater. Interfaces 2015, 7, 10283−10292

Chart 2. Plausible Mechanism for the Formation of BTD3

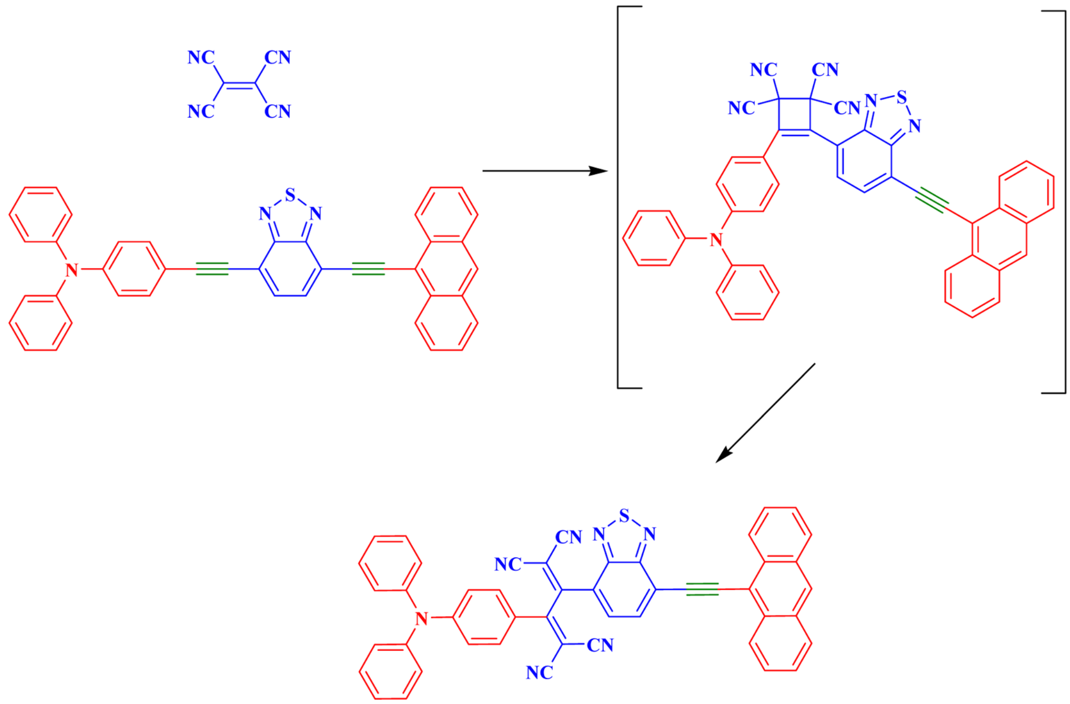

Sonogashira cross-coupling of 4-ethynyltriphenylamine with 4,7-dibromobenzo[*c*][1,2,5]thiadiazole following earlier reports.[45] The Pd-catalyzed Sonogashira cross-coupling reaction of BTD1 with 9-ethylanthracene (**4**) resulted in BTD2 in 74% yield.[45]

The [2 + 2] cycloaddition−retroelectrocyclization reaction of tetracyanoethene (**5**) with BTD2 in dichloromethane at 40 °C resulted in BTD3 in 70% yield. The purification of BTD3 was achieved by column chromatography. The exclusive formation of mono-TCNE-substituted product could be justified on the basis of a plausible mechanism of [2 + 2] cycloaddition−retroelectrocyclization reaction of tetracyanoethene (Supporting Information (SI) Chart S1) and the earlier work performed (SI Chart S2).[46] The [2 + 2] cycloaddition−retroelectrocyclization reaction of **5** with ANT-BTD resulted in recovery of the starting material (SI Chart S2). This indicates that acetylene linkage between the anthracene donor and BTD acceptor unit is not susceptible to [2 + 2] cycloaddition−retroelectrocyclization reaction and hence results is mono-TCNE-substituted BTD3. The plausible mechanism for the formation of BTD3 is shown in Chart 2. The BTD3 was well-characterized by ^{1}H and ^{13}C NMR and HRMS techniques.

The stability of organic chromophore at elevated temperatures is significant for practical applications. In order to determine the thermal stability of BTD3 thermogravimetric analysis (TGA) was carried out at a heating rate of 10 °C min^{-1}, under nitrogen atmosphere (SI Figure S7). The decomposition temperature (T_d) for 5% weight loss for BTD3 is 469 °C. The thermal stability shown in SI Table S1 indicates that the incorporation of the TCNE unit in BTD3 results in better thermal stability compared to BTD2.

Optical and Electrochemical Properties. The optical absorption spectra of BTD3 in the UV−visible region are shown in Figure 1, and the photonic parameters are

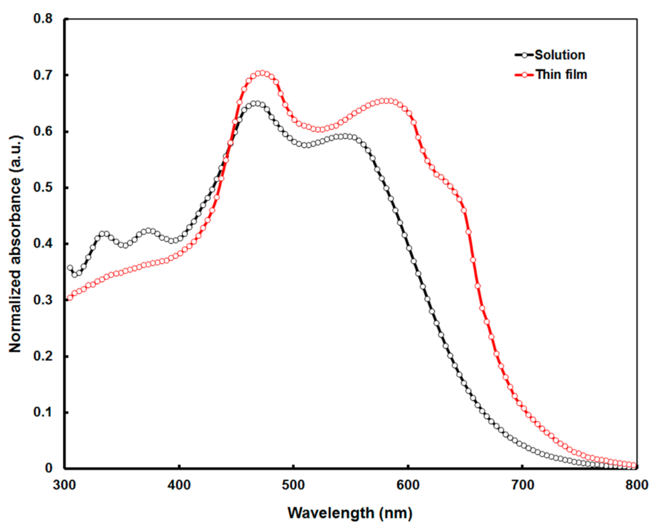

Figure 1. Normalized optical absorption spectra of BDT3 in solution and thin film.

summarized in Table 1. It exhibits two distinct bands in the absorption spectrum in dichloromethane (DCM) solution. One band with absorption peak around 467 nm results from localized π−π* transitions, and the second band with absorption peak around 545 nm is attributed to intramolecular charge transfer (ICT) between donor and acceptor moieties present in the small molecule. Compared to the absorption

DOI: 10.1021/acsami.5b02250
ACS Appl. Mater. Interfaces 2015, 7, 10283−10292

Table 1. Optical and Electrochemical Properties of BDT3.[a]

compd	λ_{abs} (nm) (ε (10^4 M^{-1} cm^{-1}))	λ_{abs} (nm) film	optical gap (eV)	calcd gap (eV)	E_{ox} (V)	E_{red} (V)	electrochemical gap (eV)
BDT3	545 (5.923), 467 (6.459)	473, 585	1.68	2.28	1.31[b]	−0.43, −0.79, −1.67	1.84

[a]Recorded by cyclic voltammetry, in 0.1 M solution of $TBAPF_6$ in DCM at 100 mV s^{-1} scan rate versus SCE electrode. [b]For the irreversible redox process, the peak potential is quoted.

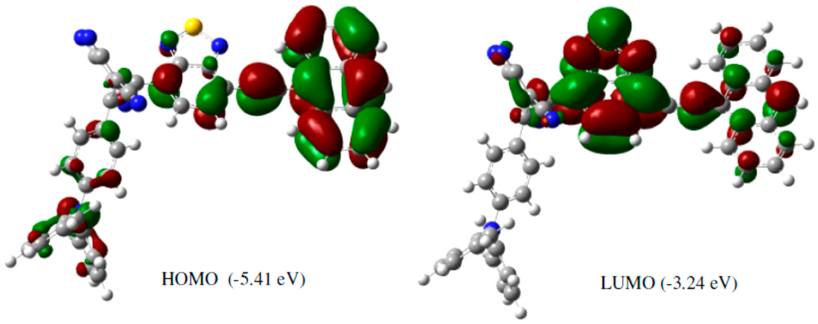

Figure 2. HOMO and LUMO orbitals of BTD3 at the B3LYP/6-31G** level for C, N, S, and H.

spectra in solution, the thin film spectrum was broadened and red-shifted with an absorption peak around 580 nm of the ICT band. Additionally, a vibronic shoulder peak around 640 nm was also observed, which indicates that the SM has stronger intermolecular $\pi-\pi$ packing interactions between molecular backbones in the solid state.[47,48] Moreover, the SM possesses a broad absorption coverage ranging from 300 to 750 nm in thin film suggesting that two electron withdrawing acceptors have strong interactions with the aryl donor through the π-linkers. The optical bandgap estimated from the onset absorption edge in thin film is about 1.68 eV. Inspection of Chart 1 shows that optical bandgap values of symmetrical BTDs of the type D−π−A−π−D are 2.24 eV (TPA−BTD) and 2.14 eV (ANT−BTD). The unsymmetrical BTD of the type D1−π−A−π−D2 exhibits an optical bandgap value of 2.20 eV. The results clearly reflect that unsymmetrical BTD3 of the type D−A−A′−π−D with TCBD linkages shows efficient tuning of the optical bandgap as desired for BHJ organic solar cell application.[45]

The electrochemical properties of BTD3 were explored by the cyclic voltammetric analysis in dichloromethane (DCM) solution using tetrabutylammonium hexafluorophosphate ($TBAPF_6$) as supporting electrolyte. The cyclic voltammogram is presented in SI Figure S8, and the data are listed in Table 1. The aryl-substituted BTD3 exhibits two reversible reduction waves corresponding to the TCBD unit at −0.43 and −0.79 V, and a third reversible reduction wave at −1.67 V due to the BTD acceptor. The irreversible oxidation peak corresponds to the oxidation potential of the aryl unit in BTD3. The HOMO and LUMO energy levels of the BTD3 are HOMO/LUMO = $-q(E_{onset} + 4.4)$ eV;[49] E_{onset} (1.16 V) is the onset potential (oxidation and reduction). The onset oxidation potential and reduction potential are 1.16 and −0.79 V, respectively (SI Figure S8). The HOMO and LUMO levels are estimated as −5.56 and −3.61 eV, respectively with a corresponding electrochemical band gap of about 1.95 eV. Considering that $PC_{71}BM$ has HOMO and LUMO levels of around −6.0 and −4.1 eV, respectively, as acceptor for fabrication for organic solar cells, its energy levels will be compatible for efficient photoinduced charge transfer from BDT3 donor to $PC_{71}BM$ acceptor, when used as blended active layer for organic BHJ solar cells. Moreover, a deeper HOMO energy level is beneficial for the high open circuit voltages of fabricated BHJ organic solar cells.

Theoretical Calculations. In order to explore the electronic structure of BTD3, density functional theory (DFT) calculation was performed at the B3LYP/6-31G** level. The contours of the HOMO and LUMO of BTD3 are shown in Figure 2. The computational results indicate the following: (a) The HOMO orbital in BTD3 is localized over anthracene and the benzo of the BTD, whereas the LUMO is delocalized over the benzothiadiazole and the 1,1,4,4-tetracyanobuta-1,3-diene (TCBD) unit. (b) The calculated HOMO and LUMO energies of the ground state optimized geometry of the BTD3 were −5.41 and −3.24 eV, respectively. The calculated HOMO and LUMO gap of BTD3 is 2.28 eV. (c) The optimized geometry of BTD3 shows that the ethynyl linked anthracene donor unit adopts a planar orientation with the BTD core as desired for extended electronic delocalization and efficient $\pi-\pi$ stacking of adjacent molecules in films (SI Figure S9).

Photovoltaic Properties. BHJ organic solar cells were fabricated with BTD3 as the electron donor and $PC_{71}BM$ as electron acceptor. $PC_{71}BM$ instead of $PC_{61}BM$ was chosen as the electron acceptor due to its stronger absorption in the visible region.[50] Photovoltaic properties were investigated using the ITO/PEDOT:PSS/BDT3:$PC_{71}BM$/Al device structure. The active layer is a blend of BDT3 and $PC_{71}BM$, spin-coated from THF solution with different weight ratios. The performance of the organic solar cells based on this molecule is very sensitive to the weight ratio of donor to acceptor, and a donor to acceptor ratio of 1:2 by weight and a thickness of 90−95 nm were optimized to give the best performance. The photovoltaic parameters for the organic solar cells based on BDT3:$PC_{71}BM$ with different weight ratios, i.e., 1:05, 1:1, 1:2, and 1:2.5, are complied in SI Table S3a. The current−voltage ($J-V$) characteristics of the optimized OSC device under illumination of AM 1.5 G (100 mW/cm^2) is shown in Figure 3a, and the photovoltaic parameters are summarized in Table 2.

The optimized device based on BDT3:$PC_{71}BM$ (1:2) gave a PCE of 3.15% with J_{sc} = 7.45 mA/cm^2, V_{oc} = 0.94 V, and FF = 0.45. In order to improve the PCE of the solar cell, we have used 1-chloronaphthalene (CN) as solvent additive to prepare the BHJ active layer. We have added different volume

DOI: 10.1021/acsami.5b02250
ACS Appl. Mater. Interfaces 2015, 7, 10283−10292

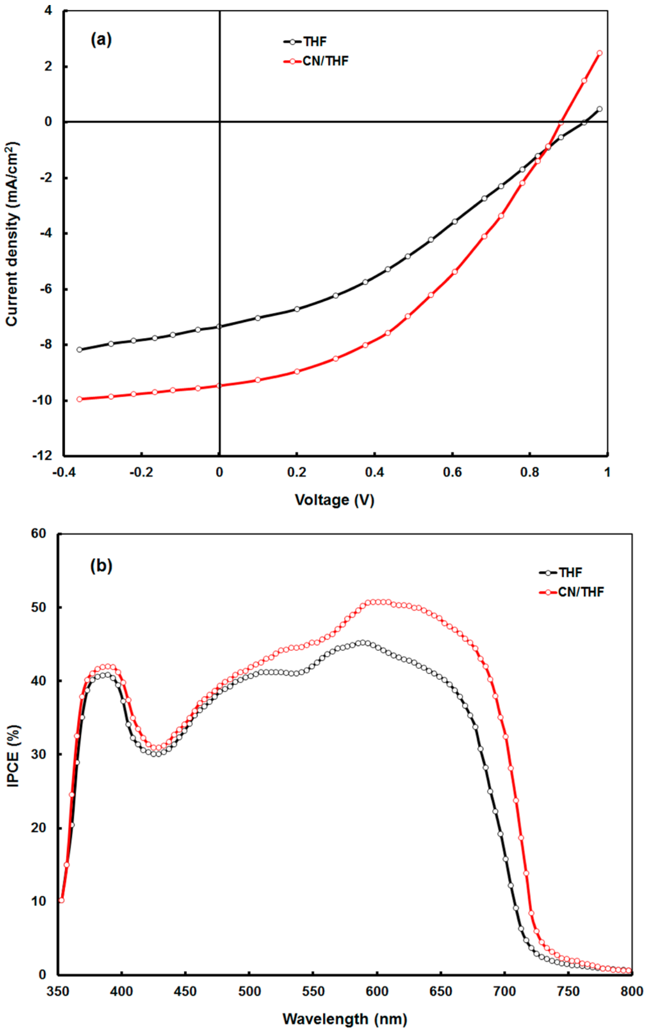

Figure 3. (a) Current −voltage ($J-V$) characteristics under illumination (AM 1.5, 100 mW/cm^2) and (b) IPCE spectra of organic solar cells.

Table 2. Photovoltaic Parameters of BHJ Organic Solar Cells Based on BTD3:PC$_{71}$BM (1:2) Blends Processed with THF and CN(3vol.%)/THF

active layer	J_{sc} (mA/cm^2)	V_{oc} (V)	FF	PCE (%)	μ_e/μ_h
BTD3:PC$_{71}$BM[a]	7.45	0.94	0.45	3.15	19
BTD3:PC$_{71}$BM[b]	9.48	0.90	0.54	4.61	4.28

[a]Processed with THF. [b]Processed with CN(3vol.%)/THF.

concentrations (1, 2, 3, and 4 vol. %) of the CN into the host THF solvent and tested the device performance. The photovoltaic performance of the device summarized in SI Table S3b shows that the optimized concentration was 3 vol. % CN/THF. The $J-V$ characteristics of the optimized organic solar cell based on the BHJ BDT3:PC$_{71}$BM (1:2) active layer processed with solvent additive is shown in Figure 3a (red color). The PCE has been further improved up to 4.61% with J_{sc} = 9.48 mA/cm^2, V_{oc} = 0.90 V, and FF = 0.54, when the BHJ active layer was processed with 3 vol. % CN/THF being used as solvent. The devices yielded high V_{oc} value, consistent with the deep HOMO energy level (−5.56 eV), since the V_{oc} for the BHJ organic solar cells is directly related with the difference in the LUMO energy level of acceptor and HOMO energy level of donor materials employed in the BHJ active layer.[51] The difference between the HOMO level of BDT3 and the LUMO level of PC$_{71}$BM is about 1.5 eV; therefore, the theoretical value of V_{oc} must be around 1.5 V, but the lower experimentally observed value may be due to the voltage losses at the interfaces between the anode and cathode. The solar cell that has been prepared from the active layer spin-coated from CN/THF exhibited PCE of 4.61%. The improvement in the PCE arose from the increase in the J_{sc} (from 7.45 to 9.48 mA/cm^2) and FF (from 0.45 to 0.54). J_{sc} strongly depends on the number of excitons generated in the active layer,[52] and the photo-response (IPCE spectra).[53] The blend film cast from CN/THF absorbed a greater fraction of incident light than the film cast from pristine THF (absorption spectra as shown in Figure 4).

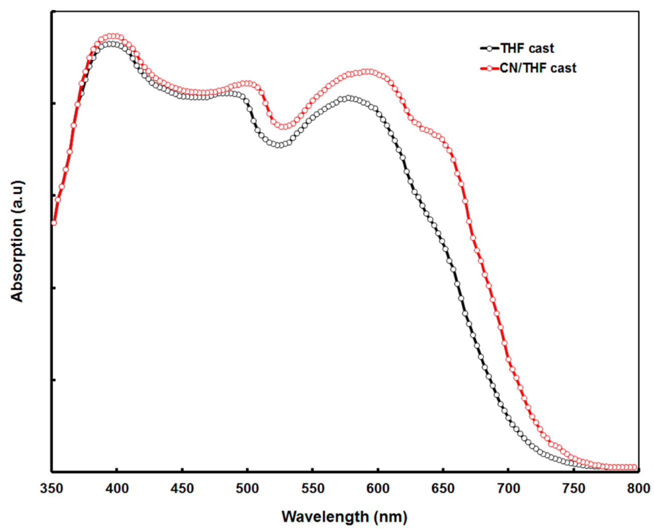

Figure 4. Optical absorption spectra of BDT3:PC$_{71}$BM (1:2) blend films cast from THF and CN/THF solvents.

The stronger absorption coefficients of the blend cast from CN/THF, which most likely increased the exciton and change generation in the device, were induced by the solvent additive.

The IPCE, which is determined by illumination with monochromatic light, is an important parameter for evaluating the photovoltaic performance of solar cells. IPCE curves of the devices based on BDT3:PC$_{71}$BM (1:2) cast with and without additive are shown in Figure 3b (red color). The THF-cast BDT3:PC$_{71}$BM-based devices exhibited a broader IPCE response in the range of 350−750 nm with a maximum of 45% at 590 nm. When the active layer was processed with CN additive, the IPCE response was further enhanced with maximum value of 52% at 605 nm. The enhanced IPCE spectrum of the device with the active layer processed with CN/THF solvent was attributed to more conversion of incident photons into the photocurrent at the absorption wavelengths corresponding to the absorption band of BDT3, consistent with the higher J_{sc} value.[54] The J_{sc} values calculated from the integration of IPCE response agrees well with the values obtained from the $J-V$ characteristics under illumination.

The photovoltaic performance of the organic BHJ solar cells are closely related with the nanomorphology of the active layer. The film morphologies of BDT3:PC$_{71}$BM (1:2) blend film cast from THF and CN/THF solvents were investigated by atomic force microscopy (AFM, in tapping mode). Figure 5 shows

DOI: 10.1021/acsami.5b02250
ACS Appl. Mater. Interfaces 2015, 7, 10283−10292

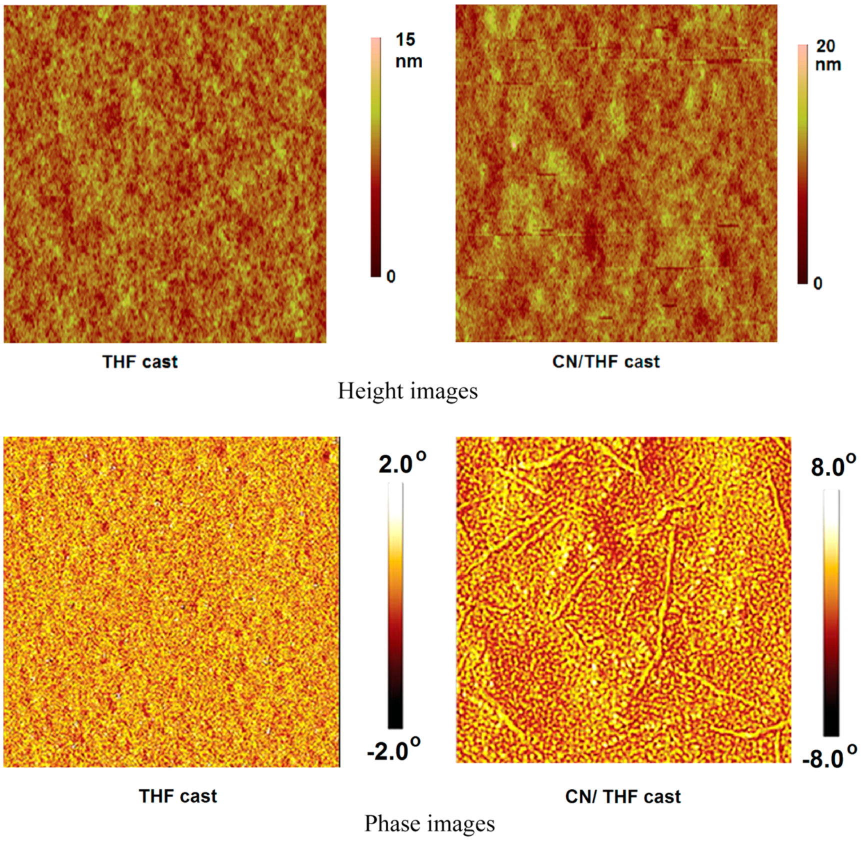

Figure 5. AFM images of BDT3:$PC_{71}BM$ blend films cast from THF and CN/THF solutions (size, 3 μm × 3 μm).

AFM height and phase images of the blend films processed with THF and CN/THF. The blend film casts from the THF solvent showed a relatively homogeneous and flat surface with a root mean squared (RMS) surface roughness of 0.54 nm and poor phase separation which was not favorable for charge transfer from BDT3 to $PC_{71}BM$, and thus limited the PCE of the resulting device. However, the spin-coated film from CN/THF has slightly more aggregated domains and a phase separated surface with larger RMS roughness of 1.90 nm. The phase separation has also been increased with the addition of CN additive. The aggregated domains may be likely originated from the enhanced intermolecular interaction of SM, during the film formation.[55,56] A higher surface roughness is expected to increase the internal light scattering and enhance the light absorption,[55,57] which is consistent with the absorption spectra displayed in Figure 5. The blend film with larger domain size suggests a good phase separation and well-connected domains, which allow efficient charge generation and charge transfer within the active layer. The improvement in the absorption was observed only in the wavelength region corresponding to the BDT3, which may be due to the close packing of BDT3 induced by CN additive as described by the XRD results. The increase in surface roughness and phase separation is favorable for exciton dissociation and interpenetrating pathways for charge transport. All of these effects enhance the value of J_{sc} and PCE for the device processed with CN/THF solvent than that exhibited by the device processed with THF only.

To get information about the molecular packing of the BDT3, the XRD patterns of the BDT3:$PC_{71}BM$ films spin-cast from THF and CN/THF were recorded and shown in Figure 6. The XRD patterns indicate that the BDT3:$PC_{71}BM$ film cast from THF exhibited a relatively weak crystalline structure with

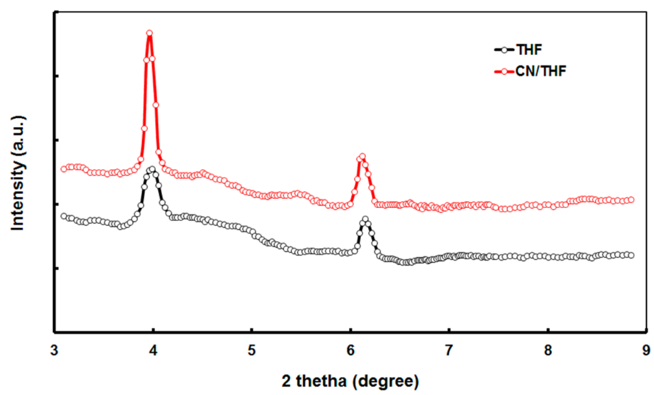

Figure 6. XRD patterns of BDT3:$PC_{71}BM$ blend films cast from THF and CN/THF solutions.

a well-defined signal (100) at $2\theta = 3.95°$ that corresponds to a d-spacing of 20.43 Å. Moreover, another signal at $2\theta = 6.12°$ was also observed, corresponding to scattering from a second order reflection. When the film was cast from CN/THF solvent, the diffraction peaks remained at the same position, but the intensity increased and narrowed. These results indicate that solvent additive improves the $\pi-\pi$ stacking structure,[58] phase separation, and crystallinity of the active layers upon these treatments, in agreement with the AFM images. The high ordered crystallites in the blend active layer enabled efficient charge transport,[59] leading to superior PCE as compared to the device processed with the active layer without solvent additive.

To gain further insight into the effect of solvent additive on the charge transport, the space charge limited current (SCLC) method was used to estimate the hole and electron mobilities of

DOI: 10.1021/acsami.5b02250
ACS Appl. Mater. Interfaces 2015, 7, 10283−10292

the active layer processed with and without CN additive, using hole and electron only devices, respectively. According to the SCLC model, current density can be expressed by the following equation:[60]

$$J = (9/8)\varepsilon\mu\left(\frac{V^2}{L^3}\right)$$

where ε and L are the permittivity of the blend film, respectively, μ is the charge carrier (hole or electron) mobility, and V is the applied voltage. Figure 7 shows the variation of the dark current of hole only devices (ITO/PEDOT:PSS/active layer/Au) with corrected bias voltage, which is determined by the built-in potential (V_{bi}) that arose from the work function difference of anode and cathode electrodes. The SCLC fitted curves are shown by the solid lines. Similar characteristics have been observed for the electron only devices (ITO/Al/active layer/Al) using the active layer. The hole mobilities for the active layer processed without and with additive are 1.34×10^{-5} and 5.56×10^{-5} cm^2/(V s), respectively. The hole mobility was enhanced significantly, but the electron mobility changed slightly (from 2.54×10^{-4} to 2.38×10^{-4} cm^2/(V s)). The increase in hole mobility can be attributed to the increase in the crystalline nature of BTD3 in the blend as confirmed from the XRD and absorption spectra data. The ratios of electron and hole mobilities in the active layer cast with and without additive are 19 and 4.28, respectively, indicating more balanced charge transport in the device based on the active layer processed with CN/THF solvent. In the case of the device processed with THF only, hole accumulation occurs in the device due to the unbalanced transport between the electron and hole; the photocurrent is space charge limited.[61]

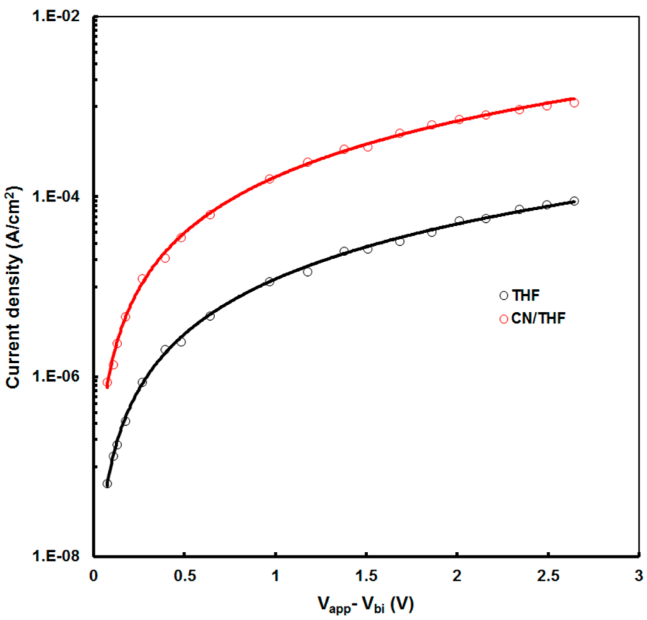

Figure 7. Current−voltage (J−V) characteristics of hole only devices. The solid lines are SCLC fitted.

It can be seen from Table 2 that the FF of the device processed with CN additive increased to 0.54 as compared to 0.45 for the device processed without CN. The improvement of FF can be partly attributed to a decrease of the series resistance (R_s) as derived from the slope of the device J−V characteristics under forward bias (under illumination), by increase of shunt resistance (R_{sh}) derived from the slope in the third quadrant of J−V characteristics. The smaller value of R_s for the device processed with CN/THF (10.13 Ω cm^2) as compared to the device processed with THF (18.17 Ω cm^2) indicates that there is favorable charge transport with the active layer processed with additive. On the other hand, the larger R_{sh} (457.12 Ω cm^2 and 346.16 Ω cm^2 for devices processed with and without CN additive) indicates reverse current density is smaller, resulting in higher FF.

We have calculated the maximum exciton generation rates (G_{max}) of the devices based on THF- and CN/THF-cast active layers, according to the method reported in the literature.[62−65] Figure 8 shows the variation of photocurrent density (J_{ph}) as a function of effective voltage (V_{eff}). Here, J_{ph} is determined as $J_{ph} = J_L - J_D$, where J_L and J_D are the current densities under illumination (100 mW/cm^2) and in the dark, respectively. The effective voltage is defined as $V_{eff} = V_o - V_{app}$, where V_o is the voltage when J_{ph} is zero ($J_L = J_D$) and V_{app} is the applied voltage. Figure 8 shows two distinct regions: one is where the J_{ph} values increase linearly with increasing V_{eff} in the low V_{eff} region, and the other is where J_{ph} saturated at a sufficiently high value of V_{eff} (i.e., V_{eff} = 1.8 V). We assume that all of the photogenerated excitons are dissociated into free charge carriers and collected by electrodes afterward in the high V_{eff} regions; the saturation photocurrent density (J_{sat}) is only limited by the total number of absorbed photons. G_{max} was estimated using $J_{sat} = qG_{max}L$, where L is the thickness of the active layer. The values of J_{sat} were estimated by asymptotic fitting of J_{ph}−V_{eff} curves. The value of J_{sat} for the device processed with CN/THF solvent increased from 87 to 104 A/m^2, thus leading to an increase in G_{max} from 6.04×10^{28} to 7.2×10^{28} m^{-3}s^{-1}. Since G_{max} is only related to the light harvesting ability of the active layer,[66,67] the enhanced G_{max} value indicates improved light harvesting efficiency and consistence with the absorption profile (Figure 4).

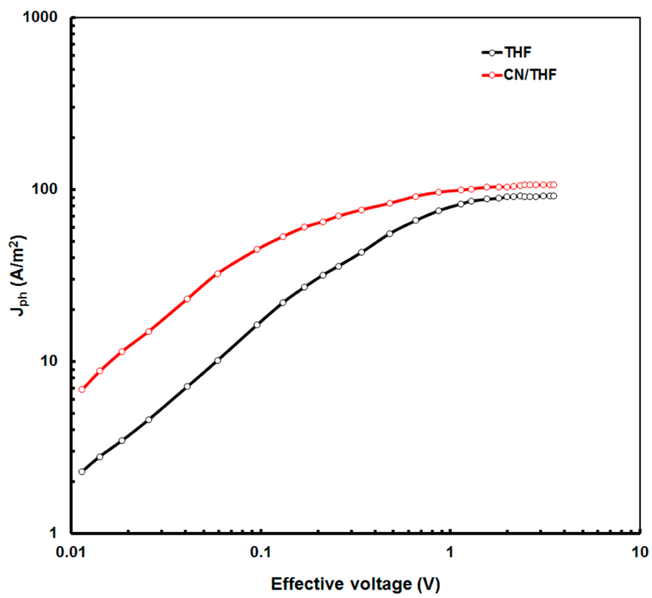

Figure 8. Photocurrent density (J_{ph}) versus effective voltage (V_{eff}) characteristics for both devices under constant incident light intensity (AM 1.5G, 100 mW/cm^2).

The exciton dissociation probability was estimated from the normalized photocurrent density (J_{ph}/J_{sat}) at short circuit

DOI: 10.1021/acsami.5b02250
ACS Appl. Mater. Interfaces 2015, 7, 10283−10292

conditions (V_{app} = 0).[68,69] The exciton dissociation probabilities for the devices based on the active layer BDT3:$PC_{71}BM$ processed with CN/THF was increased to 0.91 as compared to 0.86 for the device processed with THF-cast BDT3:$PC_{71}BM$ layer. These results indicate that more appropriate nanoscale phase separation of the active blend layer induced by the solvent additive increases the exciton dissociation probability.

4. CONCLUSION

A new low bandgap D1−A−A′−π−D2 type unsymmetrical small molecule named as BTD3 was synthesized and applied as donor along with $PC_{71}BM$ as acceptor for solution processed BHJ organic solar cells. BTD3 exhibits a deeper HOMO energy level of −5.5 eV and a LUMO level of −3.65 eV. The fabricated BHJ organic solar cell with BTD3:$PC_{71}BM$ (1:2, w/w) processed with THF and CN(3vol.%)/THF exhibits an overall PCE of 3.15% (J_{sc} = 7.45 mA/cm^2, V_{oc} = 0.94 V, and FF = 0.45) and 4.61% (J_{sc} = 9.48 mA/cm^2, V_{oc} = 0.90 V, and FF = 0.54). The enhancement in the PCE has been attributed to mainly increases in J_{sc} and FF, related to more phase separated nanoscale morphology of the active layer induced from the solvent additive. The appropriate morphology leads to enhancement in the light harvesting ability of the active layer, exciton dissociation probability, and charge transport in the device. The research work on the effect of the interfacial layer on the photovoltaic properties of the optimized devices is in progress and will be communicated later on.

■ ASSOCIATED CONTENT

Supporting Information

Text describing experimental details for BTD2 and BTD3, figures showing ^{1}H, ^{13}C NMR, and HRMS spectra of new compounds, a plausible mechanism of reaction for tetracyanoethane, a summary of earlier and present work on TCNE-BTD molecular systems, and a TGA plot, CVs, and optimized geometries of BTD3, and tables listing DFT calculation data and the electrochemical data of BTD3. The Supporting Information is available free of charge on the ACS Publications website at DOI: 10.1021/acsami.5b02250.

■ AUTHOR INFORMATION

Corresponding Authors

*(G.D.S.) E-mail: sharmagd_in@yahoo.com; gdsharma273@gmail.com.

*(R.M.) E-mail: rajneeshmisra@iiti.ac.in.

Notes

The authors declare no competing financial interest.

■ ACKNOWLEDGMENTS

R.M. thanks CSIR and DST, New Delhi for financial support.

■ REFERENCES

(1) Li, G.; Zhu, R.; Yang, Y. Polymer Solar Cells. *Nat. Photonics* **2012**, *6*, 153−161.

(2) Krebs, F. C.; Espinosa, N.; Hösel, M.; Søndergaard, R. R.; Jørgensen, M. 25th Anniversary Article: Rise to Power—OPV-Based Solar Parks. *Adv. Mater.* **2014**, *26*, 29−39.

(3) Krebs, F. C.; Hösel, M.; Corazza, M.; Roth, B.; Madsen, M. V.; Gevorgyan, S. A.; Søndergaard, R. R.; Karg, D.; Jørgensen, M. Freely Available OPV−The Fast Way to Progress. *Energy Technol.* **2013**, *1*, 378−381.

(4) Mori, T.; Nishimura, T.; Yamamoto, T.; Doi, I.; Miyazaki, E.; Osaka, I.; Takimiya, K. Consecutive Thiophene-Annulation Approach to π-Extended Thienoacene-Based Organic Semiconductors with [1]Benzothieno[3,2-*b*][1]benzothiophene (BTBT) Substructure. *J. Am. Chem. Soc.* **2013**, *135*, 13900−13913.

(5) Tsao, H. N.; Cho, D.; Andreasen, J. W.; Rouhanipour, A.; Breiby, D. W.; Pisula, W.; Müllen, K. The Influence of Morphology on High-Performance Polymer Field-Effect Transistors. *Adv. Mater.* **2009**, *21*, 209−212.

(6) Zhang, W.; Smith, J.; Watkins, S. E.; Gysel, R.; McGehee, M.; Salleo, A.; Kirkpatrick, J.; Ashraf, S.; Anthopoulos, T.; Heeney, M. Indacenodithiophene Semiconducting Polymers for High-Performance, Air-Stable Transistors. *J. Am. Chem. Soc.* **2010**, *132*, 11437−11439.

(7) He, Z.; Zhong, C.; Su, S.; Xu, M.; Wu, H.; Cao, Y. Enhanced Power-Conversion Efficiency in Polymer Solar Cells Using an Inverted Device Structure. *Nat. Photonics* **2012**, *6*, 591−595.

(8) Nelson, J. Polymer:Fullerene Bulk Heterojunction Solar Cells. *Mater. Today* **2011**, *14*, 462−470.

(9) Dou, L.; You, J.; Hong, Z.; Xu, Z.; Li, G.; Street, R. A.; Yang, Y. 25th Anniversary Article: A Decade of Organic/Polymeric Photovoltaic Research. *Adv. Mater.* **2013**, *25*, 6642−6671.

(10) Po, R.; Bernardi, A.; Calabrese, A.; Carbonera, C.; Corso, G.; Pellegrino, A. From Lab to Fab: How Must the Polymer Solar Cell Materials Design Change?—An Industrial Perspective. *Energy Environ. Sci.* **2014**, *7*, 925−943.

(11) Hösel, M.; Søndergaard, R. R.; Angmo, D.; Krebs, F. C. Comparison of Fast Roll-to-Roll Flexographic, Inkjet, Flatbed, and Rotary Screen Printing of Metal Back Electrodes for Polymer Solar Cells. *Adv. Eng. Mater.* **2013**, *15*, 995−1001.

(12) Mishra, A.; Bäuerle, P. Small Molecule Organic Semiconductors on the Move: Promises for Future Solar Energy Technology. *Angew. Chem., Int. Ed.* **2012**, *51*, 2020−2067.

(13) Son, H. J.; Carsten, B.; Jung, I. H.; Yu, L. Overcoming Efficiency Challenges in Organic Solar Cells: Rational Development of Conjugated Polymers. *Energy Environ. Sci.* **2012**, *5*, 8158−8170.

(14) Beaujuge, P. M.; Fréchet, J. M. J. Molecular Design and Ordering Effects in π-Functional Materials for Transistor and Solar Cell Applications. *J. Am. Chem. Soc.* **2011**, *133*, 20009−20029.

(15) Walker, B.; Kim, C.; Nguyen, T.-Q. Small Molecule Solution-Processed Bulk Heterojunction Solar Cells. *Chem. Mater.* **2010**, *23*, 470−482.

(16) Bai, H.; Cheng, P.; Wang, Y.; Ma, L.; Li, Y.; Zhua, D.; Zhan, X. A Bipolar Small Molecule Based on Indacenodithiophene and Diketopyrrolopyrrole for Solution Processed Organic Solar Cells. *J. Mater. Chem. A* **2014**, *2*, 778−784.

(17) Lin, Y.; Dam, H. F.; Andersen, T. R.; Bundgaard, E.; Fu, W.; Chen, H.; Krebs, F. C.; Zhan, X. Ambient Roll-to-Roll Fabrication of Flexible Solar Cells Based on Small Molecules. *J. Mater. Chem. C* **2013**, *1*, 8007−8010.

(18) Nikiforov, M. P.; Lai, B.; Chen, W.; Chen, S.; Schaller, R. D.; Strazalka, J.; Maser, J.; Darling, S. B. Detection and Role of Trace Impurities in High-Performance Organic Solar Cells. *Energy Environ. Sci.* **2013**, *6*, 1513−1520.

(19) Min, J.; Luponosov, Y. N.; Gerl, A.; Polinskaya, M. S.; Peregudova, S. M.; Dmitryakov, P. V.; Bakirov, A. V.; Shcherbina, M. A.; Chvalun, S. N.; Grigorian, S.; Busies, N. K.; Ponomarenko, S. A.; Ameri, T.; Brabec, C. J. Alkyl Chain Engineering of Solution-Processable Star-Shaped Molecules for High-Performance Organic Solar Cells. *Adv. Energy Mater.* **2014**, *4*, 1301234−1301243.

(20) Leliège, A.; Blanchard, P.; Rousseau, T.; Roncali, J. Triphenylamine/Tetracyanobutadiene-Based D-A-D π-Conjugated Systems as Molecular Donors for Organic Solar Cells. *Org. Lett.* **2011**, *13*, 3098−3101.

(21) Shang, H.; Fan, H.; Liu, Y.; Hu, W.; Li, Y.; Zhan, X. A Solution-Processable Star Shaped Molecule for High-Performance Organic Solar Cells. *Adv. Mater.* **2011**, *23*, 1554−1557.

(22) Shen, S.; Jiang, P.; He, C.; Zhang, J.; Shen, P.; Zhang, Y.; Yi, Y.; Zhang, Z.; Li, Z.; Li, Y. Solution-Processable Organic Molecule Photovoltaic Materials with Bithienyl-benzodithiophene Central Unit and Indenedione End Groups. *Chem. Mater.* **2013**, *25*, 2274−2281.

DOI: 10.1021/acsami.5b02250
ACS Appl. Mater. Interfaces 2015, 7, 10283−10292

(23) Lin, Y.; Ma, L.; Li, Y.; Liu, Y.; Zhu, D.; Zhan, X. A Solution-Processable Small Molecule Based on Benzodithiophene and Diketopyrrolopyrrole for High-Performance Organic Solar Cells. *Adv. Energy Mater.* **2013**, *3*, 1166−1170.
(24) Sun, Y.; Welch, G. C.; Leong, W. L.; Takacs, C. J.; Bazan, G. C.; Heeger, A. J. Solution-Processed Small-Molecule Solar Cells with 6.7% Efficiency. *Nat. Mater.* **2012**, *11*, 44−48.
(25) Liu, Y.; Yang, Y.; Chen, C.-C.; Chen, Q.; Dou, L.; Hong, Z.; Li, G.; Yang, Y. Solution-Processed Small Molecules Using Different Electron Linkers for High-Performance Solar Cells. *Adv. Mater.* **2013**, *25*, 4657−4662.
(26) Zhou, J.; Wan, X.; Liu, Y.; Zou, Y.; Li, Z.; He, G.; Long, G.; Ni, W.; Li, C.; Su, X.; Chen, Y. Small Molecules Based on Benzo[1,2-*b*:4,5-*b*′]dithiophene Unit for High-Performance Solution-Processed Organic Solar Cells. *J. Am. Chem. Soc.* **2012**, *134*, 16345−16351.
(27) Li, W.; Kelchtermans, M.; Wienk, M. M.; Janssen, R. A. J. Effect of Structure on the Solubility and Photovoltaic Properties of Bis-diketopyrrolopyrrole Molecules. *J. Mater. Chem. A* **2013**, *1*, 15150−15157.
(28) Zhou, J.; Zou, Y.; Wan, X.; Long, G.; Zhang, Q.; Ni, W.; Liu, Y.; Li, Z.; He, G.; Li, C.; Kan, B.; Li, M.; Chen, Y. Solution-Processed and High-Performance Organic Solar Cells Using Small Molecules with a Benzodithiophene Unit. *J. Am. Chem. Soc.* **2013**, *135*, 8484−8487.
(29) Gupta, V.; Kyaw, A. K.; Wang, D.; Chand, S.; Bazan, G. C.; Heeger, A. J. Barium: An Efficient Cathode Layer for Bulk-Heterojunction Solar Cells. *Sci. Rep.* **2013**, *3*, No. 1965.
(30) Kyaw, A. K.; Wang, D.; Wynands, D.; Zhang, J.; Nguyen, T. Q.; Bazan, G. C.; Heeger, A. J. Improved Light Harvesting and Improved Efficiency by Insertion of an Optical Spacer (ZnO) in Solution-Processed Small-Molecule Solar Cells. *Nano Lett.* **2013**, *13*, 3796−3801.
(31) Kyaw, A. K.; Wang, D.; Gupta, V.; Leong, W. L.; Ke, L.; Bazan, G. C.; Heeger, A. J. Intensity Dependence of Current−Voltage Characteristics and Recombination in High-Efficiency Solution-Processed Small-Molecule Solar Cells. *ACS Nano* **2013**, *7*, 4569−4577.
(32) Liu, Y.; Chen, C. C.; Hong, Z.; Gao, J.; Yang, Y. M.; Zhou, H.; Dou, L.; Li, G.; Yang, Y. Solution-Processed Small-Molecule Solar Cells: Breaking the 10% Power Conversion Efficiency. *Sci. Rep.* **2013**, *3*, No. 3356.
(33) Kan, B.; Zhang, Q.; Li, M.; Wan, X.; Ni, W.; Long, G.; Wang, Y.; Yang, X.; Feng, H.; Chen, Y. Solution-Processed Organic Solar Cells Based on Dialkylthiol-Substituted Benzodithiophene Unit with Efficiency near 10%. *J. Am. Chem. Soc.* **2014**, *136*, 15529−15532.
(34) Zhang, Q.; Kan, B.; Liu, F.; Long, G.; Wan, X.; Chen, X.; Zuo, Y.; Ni, W.; Zhang, H.; Li, M.; Hu, Z.; Huang, F.; Cao, Y.; Liang, Z.; Zhang, M.; Russell, T. P.; Chen, Y. Small-Molecule Solar Cells with Efficiency Over 9%. *Nat. Photonics* **2015**, *9*, 35−41.
(35) Ko, H. M.; Choi, H.; Paek, S.; Kim, K.; Song, K.; Lee, J. K.; Ko, J. Molecular Engineering of Push−Pull Chromophore for Efficient Bulk-Heterojunction Morphology in Solution Processed Small Molecule Organic Photovoltaics. *J. Mater. Chem.* **2011**, *21*, 7248−7253.
(36) So, S.; Choi, H.; Kim, C.; Cho, N.; Ko, H. M.; Lee, J. K.; Ko, J. Novel Symmetric Squaraine Chromophore Containing Triphenylamine for Solution Processed Small Molecule Bulk Heterojunction Solar Cells. *Sol. Energy Mater. Sol. Cells* **2011**, *95*, 3433−3441.
(37) So, S.; Choi, H.; Ko, H. M.; Kim, C.; Paek, S.; Cho, N.; Song, K.; Lee, J. K.; Ko, J. Novel Unsymmetrical Push−Pull Squaraine Chromophores for Solution Processed Small Molecule Bulk Heterojunction Solar Cells. *Sol. Energy Mater. Sol. Cells* **2012**, *98*, 224−232.
(38) Cho, M. J.; Seo, J.; Oh, H. S.; Jee, H.; Kim, W. J.; Kim, K. H.; Hoang, M. H.; Choi, D. H.; Prasad, P. N. Tricyanofuran-Based Donor−Acceptor Type Chromophores for Bulk Heterojunction Organic Solar Cells. *Sol. Energy Mater. Sol. Cells* **2012**, *98*, 71−77.
(39) Chen, Y.-H.; Lin, L.-Y.; Lu, C.-W.; Lin, F.; Huang, Z.-Y.; Lin, H.-W.; Wang, P.-H.; Liu, Y.-H.; Wong, K.-T.; Wen, J.; Miller, D. J.; Darling, S. B. Vacuum-Deposited Small-Molecule Organic Solar Cells with High Power Conversion Efficiencies by Judicious Molecular Design and Device Optimization. *J. Am. Chem. Soc.* **2012**, *134*, 13616−13623.
(40) Ito, K.; Suzuki, T.; Sakamoto, Y.; Kubota, D.; Inoue, Y.; Sato, F.; Tokito, S. Oligo(2,6-anthrylene)s: Acene−Oligomer Approach for Organic Field-Effect Transistors. *Angew. Chem., Int. Ed.* **2003**, *42*, 1159−1162.
(41) Ando, S.; Nishida, J.-I.; Fujiwara, E.; Tada, H.; Inoue, Y.; Tokito, S.; Yamashita, Y. Novel p- and n-Type Organic Semiconductors with an Anthracene Unit. *Chem. Mater.* **2005**, *17*, 1261−1264.
(42) Rathgeber, S.; de Toledo, D. B.; Birckner, E.; Hoppe, H.; Egbe, D. A. M. Intercorrelation between Structural Ordering and Emission Properties in Photoconducting Polymers. *Macromolecules* **2010**, *43*, 306−315.
(43) Sonar, P.; Singh, S. P.; Williams, E. L.; Li, Y.; Soha, M. S.; Dodabalapur, A. Furan Containing Diketopyrrolopyrrole Copolymers: Synthesis, Characterization, Organic Field Effect Transistor Performance and Photovoltaic Properties. *J. Mater. Chem.* **2012**, *22*, 4425−4435.
(44) Almeataq, M. S.; Yi, H.; Al-Faifi, S.; Alghamdi, A. A. B.; Iraqi, A.; Scarratt, N. W.; Wang, T.; Lidzey, D. G. Anthracene-Based Donor−Acceptor Low Band Gap Polymers for Application in Solar Cells. *Chem. Commun. (Cambridge, U. K.)* **2013**, *49*, 2252−2254.
(45) Gautam, P.; Maragani, R.; Misra, R. Aryl-Substituted Symmetrical and Unsymmetrical Benzothiadiazoles. *RSC Adv.* **2015**, *5*, 18288−18294.
(46) Kivala, M.; Diederich, F. Acetylene-Derived Strong Organic Acceptors for Planar and Nonplanar Push−Pull Chromophores. *Acc. Chem. Res.* **2009**, *42*, 235−248.
(47) Lin, L. Y.; Chen, Y. H.; Huang, Z. Y.; Lin, H. W.; Chou, S. H.; Lin, F.; Chen, C. W.; Liu, Y. H.; Wang, K. T. A Low-Energy-Gap Organic Dye for High-Performance Small-Molecule Organic Solar Cells. *J. Am. Chem. Soc.* **2011**, *133*, 15822−15825.
(48) Lee, J. K.; Jeong, B. S.; Kim, J.; Kim, C.; Ko, J. Synthesis and Photochemical Characterization of Fumaronitrile-Based Organic Semiconductor and Its Use in Solution-Processed Small Molecule Organic Solar Cells. *J. Photochem. Photobiol., A* **2013**, *251*, 25−32.
(49) Zhang, H.; Wan, X.; Xue, X.; Li, Y.; Yu, A.; Chen, Y. Selective Tuning of the HOMO−LUMO Gap of Carbazole-Based Donor−Acceptor−Donor Compounds Toward Different Emission Colors. *Eur. J. Org. Chem.* **2010**, 1681−1687.
(50) Yamanari, T.; Taima, T.; Sakai, J.; Saito, K. Highly Efficient Organic Thin-Film Solar Cells Based on Poly(3-hexylthiophene) and Soluble C70 Fullerene Derivative. *Jpn. J. Appl. Phys.* **2008**, *47*, 1230−1233.
(51) Dou, L.; You, J.; Yang, J.; Chen, C.-C.; He, Y.; Murase, S.; Moriarty, T.; Emery, K.; Li, G.; Yang, Y. Tandem Polymer Solar Cells Featuring a Spectrally Matched Low-Bandgap Polymer. *Nat. Photonics* **2012**, *6*, 180−185.
(52) Zhou, H.; Yang, L.; Wei, Y. Rational Design of High Performance Conjugated Polymers for Organic Solar Cells. *Macromolecules* **2012**, *45*, 607−632.
(53) Park, S. H.; Roy, A.; Beaupré, S.; Cho, S.; Coates, N.; Moon, J. S.; Moses, D.; Leclerc, M.; Lee, K.; Heeger, A. J. Bulk Heterojunction Solar Cells with Internal Quantum Efficiency Approaching 100%. *Nat. Photonics* **2009**, *3*, 297−302.
(54) van der Poll, T. S.; Love, J. A.; Nguyen, T.-Q.; Bazan, G. C. Non-Basic High-Performance Molecules for Solution-Processed Organic Solar Cells. *Adv. Mater.* **2012**, *24*, 3646−3649.
(55) Shi, Q.; Cheng, P.; Li, Y.; Zhan, X. A Solution Processable D−A−D Molecule Based on Thiazolothiazole for High Performance Organic Solar Cells. *Adv. Energy Mater.* **2012**, *2*, 63−67.
(56) Kyaw, A. K.; Wang, D.; Luo, C.; Cao, Y.; Nguyen, T. Q.; Bazan, G. C.; Heerger, A. J. Effects of Solvent Additives on Morphology, Charge Generation, Transport, and Recombination in Solution-Processed Small-Molecule Solar Cells. *Adv. Energy Mater.* **2014**, *4*, 1301469−1301477.
(57) Kim, Y. J.; Lee, G. B.; Jeon, C. W.; Kim, Y. H.; Chung, D. S.; Park, C. E. A Push-Pull Organic Semiconductor with Efficient

DOI: 10.1021/acsami.5b02250
ACS Appl. Mater. Interfaces 2015, 7, 10283−10292

Intramolecular Charge Transfer for Solution Processed Small Molecule Solar Cells. *RSC Adv.* **2015**, *5*, 3435−3442.
(58) Huang, J.; Jia, H.; Li, L.; Lu, Z.; Zhang, W.; He, W.; Jiang, B.; Tang, A.; Tan, Z.; Zhan, C.; Li, Y.; Yao, J. Fine-Tuning Device Performances of Small Molecule Solar Cells via the More Polarized DPP-Attached Donor Units. *Phys. Chem. Chem. Phys.* **2012**, *14*, 14238−14242.
(59) Kim, D. H.; Ayzner, A. L.; Appleton, A. L.; Schmidt, K.; Mei, J.; Toney, M. F.; Bao, Z. Comparison of the Photovoltaic Characteristics and Nanostructure of Fullerenes Blended with Conjugated Polymers with Siloxane-Terminated and Branched Aliphatic Side Chains. *Chem. Mater.* **2013**, *25*, 431−440.
(60) Melzer, C.; Koop, E. J.; Mihailetchi, V. D.; Blom, P. W. M. Hole Transport in Poly(phenylenevinylene)/methanofullerene Bulk Heterojunction Solar Cells. *Adv. Funct. Mater.* **2004**, *14*, 865−870.
(61) Moule, A. J.; Meerholz, K. Controlling Morphology in Polymer−Fullerene Mixtures. *Adv. Mater.* **2008**, *20*, 240−245.
(62) Chen, F. C.; Wu, J. L.; Lee, C. L.; Hong, Y.; Kuo, C. H.; Huang, M. H. Plasmonic-Enhanced Polymer Photovoltaic Devices Incorporating Solution-Processable Metal Nanoparticles. *Appl. Phys. Lett.* **2009**, *95*, No. 013305.
(63) Wu, J. L.; Chen, F. C.; Hsiao, Y. S.; Chien, F. C.; Chen, P.; Kuo, C. H.; Huang, M. H.; Hus, C. S. Surface Plasmonic Effects of Metallic Nanoparticles on the Performance of Polymer Bulk Heterojunction Solar Cells. *ACS Nano* **2011**, *5*, 959−967.
(64) Mihailetchi, V. D.; Koster, L. J. A.; Hummelen, J. C.; Blom, P. W. M. Photocurrent Generation in Polymer−Fullerene Bulk Heterojunctions. *Phys. Rev. Lett.* **2004**, *93*, No. 216601.
(65) Mihailetchi, V. D.; Xie, H. X.; de Boer, B.; Koster, L. J. A.; Blom, P. W. M. Charge Transport and Photocurrent Generation in Poly(3-hexylthiophene):Methanofullerene Bulk-Heterojunction Solar Cells. *Adv. Funct. Mater.* **2006**, *16*, 699−708.
(66) Lu, L.; Luo, Z.; Xu, T.; Yu, L. Cooperative Plasmonic Effect of Ag and Au Nanoparticles on Enhancing Performance of Polymer Solar Cells. *Nano Lett.* **2013**, *13*, 59−64.
(67) Shrotriya, V.; Yao, Y.; Li, G.; Yang, Y. Effect of Self-Organization in Polymer/Fullerene Bulk Heterojunctions on Solar Cell Performance. *Appl. Phys. Lett.* **2006**, *89*, No. 063505.
(68) Koster, L. J. A.; Mihailetchi, V. D.; Blom, P. W. M. Bimolecular Recombination in Polymer/Fullerene Bulk Heterojunction Solar Cells. *Appl. Phys. Lett.* **2006**, *88*, No. 052104.
(69) Mandoc, M. M.; Veurman, W.; Koster, L. J. A.; de Boer, B.; Blom, P. W. M. Origin of the Reduced Fill Factor and Photocurrent in MDMO-PPV:PCNEPV All-Polymer Solar Cells. *Adv. Funct. Mater.* **2007**, *17*, 2167−2173.

DOI: 10.1021/acsami.5b02250
ACS Appl. Mater. Interfaces 2015, 7, 10283−10292